RSC Advances

PAPER

Cite this: *RSC Adv.*, 2014, **4**, 33866

PEI@Mg_2SiO_4: an efficient carbon dioxide and nitrophenol compounds adsorbing material†

Zheng-Yong Chen,[a] Hong-Wen Gao[a] and Jia-Xiang Yang*[b]

Received 25th May 2014
Accepted 3rd July 2014

DOI: 10.1039/c4ra04928d

www.rsc.org/advances

The PEI@Mg_2SiO_4 hybrid composite is readily synthesized for adsorbing carbon dioxide (CO_2) and nitrophenol compounds (NACs), in which more than 11% PEI is embedded. By the removal rate of 4-nitrophenol (10 mg L^{-1}) and the capture capacity of CO_2, the Mg^{2+} : PEI : SiO_3^{2-} optimal mole ratio of the PEI@Mg_2SiO_4 is 1 : 0.6 : 1.5. The composite shows the highest adsorption amounts of 0.94 mmol g^{-1} CO_2 at 50 °C. The heat treatment regeneration exhibits a good stability, *e.g.* the CO_2 capture capacity decreases by only 20% after four cycles, and the desorption rate of CO_2 remains more than 91%. It also exhibits a fast adsorption and high capacity for 4-nitrophenol (NP), 2,4-dinitrophenol (DNP) and 2,4,6-trinitrophenyl group (TNP). The adsorption capacity of NP, DNP and TNP is 2.40 mmol g^{-1}, 2.66 mmol g^{-1} and 4.85 mmol g^{-1} respectively, which is more than that of the conventional sorbents. This work presents the higher capacity and eco–friendly sorbent for CO_2 and nitrophenol compounds.

Inorganic–organic (IO) materials with hierarchical structures and complex morphologies assembled through "host–guest" chemistry have attracted much attention for a fundamental interest in environmental science and their potential applications in water treatment and gas remediation.[1] It is necessary to find special properties by intercalating appointed organic material into a stable inorganic matrix. Some entity frameworks in layered architectures have been utilized as ideal "hosts" that aid in the construction of multifunctional adsorbents such as layered double hydroxides,[2] layered transition metal oxides,[3] graphite, and other lamellar materials.[4,5] In particular, layered magnesium silicate has been applied in absorbing to pollutants[6] because of its high surface area,[7,8] properties of ion exchange, hydrophobic character and molecular sieves.[9]

As a guest, surfactants and block-copolymers often are used extensively in the shape-controlled synthesis of various functional materials, in which they play the role of a soft template or stabilizer.[10,11] Among the potential "guest" molecules, diverse amine species have prospective absorption of applications in heavy metal,[12] organic contamination,[13] gaseous pollutants[14] and other fields. Polyethyleneimine (PEI) can effectively adsorb pollutants due to the high amine density, accessible primary amine sites on chain ends and good water-solubility.[15] However, before being used in the absorption for pollutants, the water-soluble PEI must be processed into a solid form. Fortunately, the combination of PEI with inorganic matrix may achieve this goal.[16] For example, Deng[17] and Ting reported that the fungal biomass with PEI-grafting showed high sorption capacity for anionic Cr(VI) and Cr(III). Tailor[18] and co-workers found that the MCM-41-supported modified PEI markedly increased the SO_2 capture capacity than that of traditional adsorbents. Gao *et al.*[19] introduced an interesting study for adsorbing phenol perfectly with modified diatomite by PEI impregnating.

Owing to the burning of fossil fuels and various chemical processes, there is a large amount of emission of CO_2, which is a greenhouse gas, into the atmosphere.[20] More and more people believe that the anthropogenic emissions of greenhouse gases contribute to global warming and climate change.[21,22] Moreover, the widespread of NACs in water is a main concern that impels researchers to look for remedies.[23–26] These compounds, in particular nitrobenzene, and their transformation products in the environment occur as contaminants worldwide and are known to be hazardous to ecology and human health.[27–29] Amine-layered IO materials have been shown to be successful for the removal of CO_2 and NACs, such as amine-layered LDHs,[30] amine-functionalized mesoporous silica[31] and milli-sized calcium.[32] Currently, there are two main classes of such amine-based IO materials: (a) amines covalently bound to the support *via* the use of chemical grafting[33–35] and (b) physically impregnated into the support based on a "wet impregnation" method.[31,36–39] The sorbents mentioned above have some obvious disadvantages, involving lack of stability, relatively low efficiency, less content of functional compound, and poor regeneration stability.[40] Our previous studies indicate that the layered IO material by coprecipitation technique has a great effect on overcoming these disadvantages.[7,35,43–45] Therefore,

[a]*State Key Laboratory of Pollution Control and Resource Reuse, College of Environmental Science and Engineering, Tongji University, Shanghai 200092, China. E-mail: hwgao@tongji.edu.cn; Fax: +86-21-65988598; Tel: +86-21-65988598*

[b]*Department of Chemistry, Key Laboratory of Functional Inorganic Materials of Anhui Province, Anhui University, Hefei 230039, P. R. China. E-mail: jxyang@ahu.edu.cn; Tel: +86-551-63861279*

† Electronic supplementary information (ESI) available. See DOI: 10.1039/c4ra04928d

there is a significant and untapped opportunity to improve the adsorption characteristics by developing the PEI-layered magnesium silicate material by coprecipitation technique. The objective of this study is (1) to form a hybrid material (PEI@Mg_2SiO_4) by coprecipitation technique, (2) to utilize the high amine density and positive charge of the PEI@Mg_2SiO_4 to adsorb NACs and CO_2 and (3) to investigate their resultant adsorptions. The results indicate that the PEI@Mg_2SiO_4 is promising to capture CO_2 and adsorb NACs from wastewater decently.

Experimental section

Apparatus and materials

The infrared spectra were obtained with a Fourier transform infrared spectrometer (Model NICOLET 5700, Thermo Electron Co., USA) to indicate PEI embedded into the hybrid materials and NAC adsorbed into the sorbent. The heat weight change of the materials was performed with a thermogravimetric analyser (Model NETZSCH TG 209 F1, NETZSCH-Geratebau GmbH, Germany). A scanning electron microscope (SEM) (Model Quanta 200 FEG, FEI Co., USA) was used to measure the size and shape of the hybrid sorbents. A transmission electron microscope (TEM) (Model TECNAI G2, S-TWIN, FEI Co., USA) was used to characterize the morphology of the PEI@Mg_2SiO_4 and Mg_2SiO_4. A ζ-potential instrument (Zetasizer Nano Z, Malvern, UK) was used to determine the surface potential of the sorbents. The surface area of the materials was measured with a surface area and porosimetry analyser (Model ASAP2020, Micromeritics Co., USA). The small-angle X-ray diffraction (SAXRD) (Model D/Max-2550 PC, Japan) was recorded using CuKa radiation at a voltage of 30 kV and current of 50 mA, and the wide-angle X-ray diffraction (WAXRD) (Model Bruker D8 Advance, Germany) in the 2θ range of $\sim 10^\circ$ to 90° at 40 kV and 40 mA. The elemental analysis device (Model Vario EL III, Germany) used to determine C, N and H content of hybrid composite. A photodiode array spectrometer (Model S4100, Scinco, Korea) with the Labpro plus software (Firmware Version 060105) was used to determine the concentration of various NAC solutions.

Sodium metasilicate (Aladdin Agents, China), magnesium nitrate (Aladdin Agents, China), sodium hydroxide (Aladdin Agents, China), PEI (M.W. 600, Aladdin Agents, China), sodium chloride (Aladdin Agents, China), and hydrochloric acid (Sinopharm Chemical Reagent Co., Ltd, China) were used. The adsorption capacities of five phenolic compounds (Aladdin Agents, China) on the PEI@Mg_2SiO_4 were investigated, which was NP, DNP, TNP, *p*–cresol and *p*–chlorophenol respectively.

Synthesis of the PEI@Mg_2SiO_4 hybrid composite and Mg_2SiO_4

2.0 g of magnesium chloride hexahydrate (AR, Aladdin Reagents Co., China) was dispersed into 100 mL of deionized water and mixed with 2.0 g ethylene imine polymer (M.W. 600, 99%, Aladdin Reagents Co., China) for 10 min with an ultrasonic fragmentation device (Model JY92-II, Xinzhi Biotechnol. Co, Ltd, Ningbo, China). 100 mL of 4.3% (w/v) sodium silicate was added rapidly with stirring. After aging for 24 h, the hybrid composite was washed repeatedly with deionized water to remove the excess PEI. The PEI@Mg_2SiO_4 suspension liquid was used to dry by freeze-drying. As reference, magnesium silicate was prepared according to the same procedure. PEI@Mg_2SiO_4 and Mg_2SiO_4 powder were used to adsorb CO_2, whereas the PEI@Mg_2SiO_4 suspension liquid was used to adsorb NACs.

Adsorption of CO_2 to the PEI@Mg_2SiO_4 and Mg_2SiO_4 material

The amount of adopted CO_2 was determined by using a thermogravimetric analyzer (Model NETZSCH TG 209 F1, NETZSCH-Geratebau GmbH, Germany). In a typical measurement procedure, the sample was degassed at 150 °C for 30 min in N_2 to remove any physically adsorbed molecules. After the temperature was decreased to 25 °C, the sample was allowed to adsorb CO_2 by passing CO_2 at a flow rate of 30 mL min^{-1}, and this process was continued for 40 min.

The influences of time and temperature on the adsorption of CO_2 were tested by using a thermogravimetric analyzer (Model NETZSCH TG 209 F1, NETZSCH-Geratebau GmbH, Germany). The sample was degassed at 150 °C for 30 min in N_2 to remove any physically adsorbed molecules, after the temperature was decreased to 50 °C, the sample was allowed to adsorbed CO_2 by passing CO_2 at a flow rate of 30 mL min^{-1}, the process was continued for 40 min. The temperature of sample was adjusted from 25 °C to 100 °C. The adsorption–desorption cycling was also measured. The sample after adsorption of CO_2 was heated at 150 °C with a ramp rate of 5 °C min^{-1} in a nitrogen atmosphere, and then the sample was maintained at this temperature for 100 min to remove the adsorbed CO_2. After the temperature was decreased to 50 °C, the sample was allowed to adsorb CO_2 again by re-passing CO_2 at a flow rate of 30 mL min^{-1}. The process was continued for another 80 min, and the process was repeated for four times.

Adsorption of NACs and phenols

The adsorption capacities of the PEI@Mg_2SiO_4 to three kinds of NACs, and two kinds of phenols were determined. The 0.02% (w/v) of the PEI@Mg_2SiO_4 was added into the NACs and solutions of phenols, *e.g.* DNP from 15 to 100 mg L^{-1}, TNP from 20 to 150 mg L^{-1}, *p*-cresol from 20 to 300 mg L^{-1}, NP from 50 to 420 mg L^{-1} and *p*-chlorophenol from 60 to 600 mg L^{-1}. The PEI@Mg_2SiO_4 pollutants were mixed for 10 min by ultrasonication. After the mixtures were centrifuged, the concentrations of pollutants in the supernatants were determined by spectrophotometry.

In addition, the influences of pH, ionic strength and time on the adsorption of NP (53 mg L^{-1}), DNP (19 mg L^{-1}) and TNP (20 mg L^{-1}) on the PEI@Mg_2SiO_4 were investigated, respectively. NaCl (1 M) was used to adjust ionic strength of the liquids from 0 to 0.2 M. The sorption time was varied from 0 to 30 min, and the pH was varied from 4 to 10. In all the experiments, the pollutants in the supernatants were determined by spectrophotometry.

Results and discussion

Interaction of PEI with magnesium silicate

Our previous study indicates that the initial optimal mole ratio of Mg^{2+} : SiO_3^{2-} is 1 : 1.5 for preparing the organics-layered magnesium silicate.[6] From the interaction of PEI with *in situ* formed magnesium silicate, an embedded amount of PEI increases with the increase of SiO_3^{2-}, and then the embedded amount of PEI approaches equilibrium.[6] The hybridization obeys the Langmuir isotherm model (Fig. 1A and B), *e.g.* $1/q_e = 1/(K_a c_e q_\infty) + 1/q_\infty$,[41–44] where c_e is the equilibrium molarity of PEI in g L^{-1}, q_e is the amount of PEI binding to magnesium silicate in mg g^{-1}, q_∞ is the saturation amount of PEI in mg g^{-1} and K_a is the binding constant. The q_∞ of PEI is calculated as 0.41 g per gram of magnesium silicate, *i.e.* the content maximum of embedded PEI in the PEI@Mg_2SiO_4 approaches 29.4%, which is more than other results of previous similar studies.[19,45,46] During the growing of Mg–O–Si particles, the positively charged amino group of PEI can bind to the negatively charged Mg–O–Si ones *via* the electrical attraction. The ζ-potential of the magnesium silicate-only is determined to be −45.5 mV in aqueous media, which may be attributed to the fact that lots of OH^- in basic media are adsorbed *via* the interaction with Mg^{2+} and O–Si.[47]

However, the results of previous studies show that there is a substantial decrease in the adsorption capacity of IO-sorbent with increase in the content of embedded PEI due to partial blockage of pores by the grafted amine molecules.[46,48,49] In order to optimize the ratio of PEI in the PEI@Mg_2SiO_4, CO_2 and NP (10 mg L^{-1}) are selected as representatives to measure the optimal pollutant adsorption capacity of the different content of embedded PEI in the PEI@Mg_2SiO_4, *e.g.* 94 mg g^{-1}, 130 mg g^{-1}, 175 mg g^{-1}, 219 mg g^{-1}, 260 mg g^{-1} and 295 mg g^{-1}. As a result, the removal rates of NP are 2.50%, 2.63%, 2.07%, 2.01%, 1.98% and 0.16%, which are obtained by using the above corresponding PEI@Mg_2SiO_4 (Fig. 1C). The adsorptions of CO_2 are 0.81 mmol g^{-1}, 0.66 mmol g^{-1}, 0.35 mmol g^{-1}, 0.06 mmol, 0 mmol and 0 mmol g^{-1}, respectively (Fig. 1D). Thus, the adsorption of NP and CO_2 are maximum in the adsorbents with the Mg^{2+} : PEI : SiO_3^{2-} ratio of 1 : 0.6 : 1.5. The PEI@Mg_2SiO_4 is formed and used. The molar ratio of Mg to PEI and Si in the PEI@Mg_2SiO_4 is calculated as 1 : 0.13 : 1.3, and it was determined by element analysis and ICP.

Characterization of the PEI@Mg_2SiO_4

An initial estimate of PEI bilayer content in the PEI@Mg_2SiO_4 is obtained from infrared (IR) spectra. As shown in Fig. 2A, the Si–O absorption peak is at 1059 cm^{-1}. The absorption peaks at 2935 (C–H stretching), 2819 (C–H stretching), (1756 –NH_2 and –NH– deformation), 1472 (–NH_2 and –NH– deformation) and 1290 cm^{-1} (–NH_2 and –NH– deformation) indicate that PEI is embedded into the PEI@Mg_2SiO_4. From the elemental analysis of the PEI@Mg_2SiO_4, both 7.1% C and 3.8% N indicate that 11.4% PEI is embedded into the PEI@Mg_2SiO_4 (Table S1, ESI†). From the small-angle XRD (SAXRD) (curve 2 in Fig. 2B), the PEI@Mg_2SiO_4 composite possesses the layered structure. During the synthesis, the positively charged amino group of PEI (structured in Fig. 2B) can bind to the negatively charged Mg–O–Si particles *via* electrical attraction. The ζ-potential of Mg_2SiO_4-only is determined to be −45.5 mV in aqueous media, which may be attributed to the fact that lots of OH^- in basic media are adsorbed *via* the interaction with Mg^{2+} and O–Si.[47] After the intercalation of PEI, the ζ-potential of the PEI@Mg_2SiO_4 changes to +15.9 mV. The electrostatic interaction occurs between PEI^+ and magnesium silicate. In addition, the alkyl chain (–[CH_2–CH_2–NH]$_n$–) of PEI in length of 3.4 nm may be embedded into two Mg_2SiO_4 sheets. PEI is fixed between Mg_2SiO_4 particles in the interval of 3.9 nm (Fig. 2B).

As shown in Fig. 3, the PEI@Mg_2SiO_4 shows the sheet morphology with an average diameter of 40–60 nm (Fig. 3B), which is similar to that of Mg_2SiO_4 (Fig. 3D). However, the PEI@Mg_2SiO_4 also shows the layer structure (Fig. 3A) because two sheets of Mg_2SiO_4 are aged into the layer-by-layer material by electric attraction. Moreover, the width of silt is about 4 nm

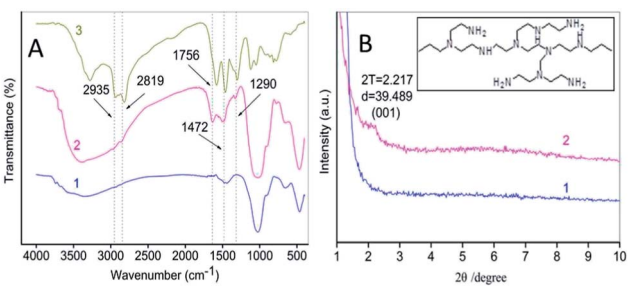

Fig. 2 IR spectra (A) of Mg_2SiO_4 (1), the PEI@Mg_2SiO_4 (2) and PEI (3) and SAXRD and (B) of Mg_2SiO_4 (1) and the PEI@Mg_2SiO_4 (2).

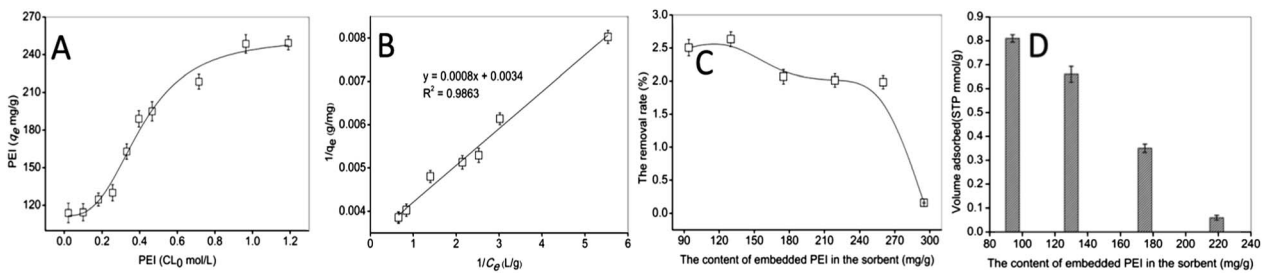

Fig. 1 Effect of PEI on the hybridization. (A) Plots q_e *versus* c_0, (B) plots c_e/q_e *versus* c_e. (C) The removal rate of NP with the different content of embedded PEI in the sorbent. (D) The adsorption of CO_2 with the different content of embedded PEI in the sorbent.

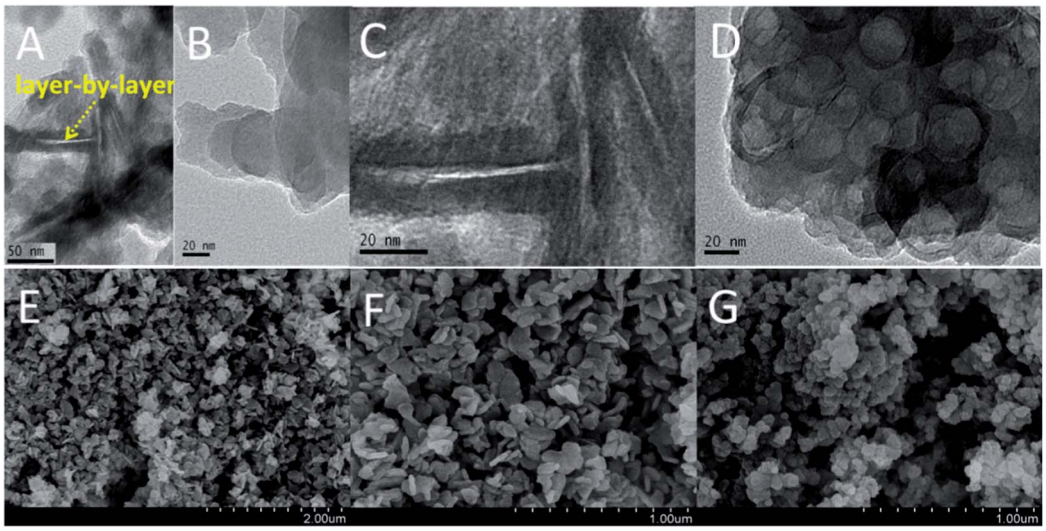

Fig. 3 TEM images of the PEI@Mg_2SiO_4 (A–C) and Mg_2SiO_4 (D). SEM of the PEI@Mg_2SiO_4 (E and F) and Mg_2SiO_4 (G).

(Fig. 3A and C), which is consistent with the SAXRD. As shown in the SEM images (Fig. 3E and F), the PEI@Mg_2SiO_4 has flaky structure with an average diameter of 60 to 100 nm, while Mg_2SiO_4 has the granule structure with the average diameter of 60–80 nm (Fig. 3G). The presence of PEI affects the stacking of lamellar Mg_2SiO_4, which is only stringed by the intermolecular action with PEI.[6] The PEI interior of the hybrid is also confirmed by EDX (Fig. S1, ESI†).

Fig. 4 illustrates the N_2 sorption isotherm and the pore-size distribution with Barrett–Joyner–Halenda method of Mg_2SiO_4 and the PEI@Mg_2SiO_4. All of the isotherms are classical type IV, which refers to the mesoporous materials. Furthermore, the isotherms have two hysteresis loops, indicating a bimodal pore size distribution in the mesoporous regions. The shapes of the two hysteresis loops are different from each other.[50] At the pressure between 0.8 and 0.9, the hysteresis loops are type H1, suggesting the presence of cylindrical mesopores.[51] The above bimodal pore-size distribution is further confirmed by the pore-size distribution in Fig. 4a and b. From the pore plots, no peak appeared in the pore, indicating the presence of irregular mesopores. The mesopores may be formed by the stacking of lamellar Mg_2SiO_4. The BET analysis of the materials indicates

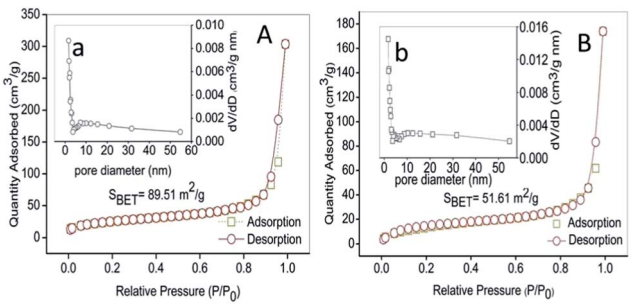

Fig. 4 N_2 absorption–desorption isotherm and pore-size distribution (inset) for Mg_2SiO_4 (A(a)) and the PEI@Mg_2SiO_4 (B(b)).

that the specific surface areas of Mg_2SiO_4 and PEI@Mg_2SiO_4 were determined to be 51.61 and 89.51 $m^2\ g^{-1}$, respectively. The increased area should be attributed to the partial impregnation of PEI into Mg_2SiO_4.

As seen in the thermogravimetric analysis (TGA) and differential thermal gravity of the PEI@Mg_2SiO_4 (Fig. S2, ESI†), the first step in the range from 40 to 200 °C is attributed to the removal of the physisorbed water and interlayer water, the second step in the range from 200 to 400 °C is due to the removal of the silicate layer, and the third step in the range from 400 to 600 °C is due to the removal of interlayer PEI. At 700 °C, the weight loss of the PEI@Mg_2SiO_4 is 33.2%, where the physisorbed water, silicate layer and interlayer PEI distribution was 15.0%, 7.9% and 10.3%, respectively, approaching that obtained from the element analysis.

Prediction of CO_2 adsorption uptakes in the PEI@Mg_2SiO_4

The CO_2 capture capacity of Mg_2SiO_4 and the PEI@Mg_2SiO_4 materials is measured at 25 °C by using a thermogravimetric analyzer. The chemisorption of CO_2 may occur through the formation of carbamate by the reaction of the secondary amine group (R_2NH) and primary amine (RNH_3) of PEI with CO_2, as shown in eqn (1) and (2) below.

$$CO_2 + 2RNH_2 \rightleftharpoons RNH_3^+\ O{-}\overset{O}{\overset{\|}{C}}NHR \quad (1)$$

$$CO_2 + 2R_2NH \rightleftharpoons R_2NH_2^+\ O{-}\overset{O}{\overset{\|}{C}}NR_2 \quad (2)$$

This suggests that CO_2 would form a weak chemical bond with the secondary amine group, and subsequently lead to the formation of carbamate zwitterions.[52] The CO_2 capture capacity on Mg_2SiO_4 is around 0.69 mmol g^{-1}, which is higher than that of the results reported.[30,53,54] The interlayer anions in Mg_2SiO_4

(ref. 47) is favourable to CO_2 capture.[31,55] The CO_2 capture capacity increases up to 0.75 mmol g^{-1} with the PEI@Mg_2SiO_4. These competing kinetic (diffusion) and thermodynamic (adsorption) effects has been observed and reported previously.[45,53] The nanopores of the PEI@Mg_2SiO_4 provide CO_2 with a diffusion path, where PEI located on the nanopore wall offers the active adsorption sites.

For CO_2 capture, any adsorbent should have not only a high sorption capacity but also fast adsorption to be energy-efficient.[56] A recent study demonstrated the high loading of amine may hamper the adsorption kinetics but increase the capacity.[57] A double-exponential model (DEM) is applied to describe the CO_2 adsorption kinetics on the PEI@Mg_2SiO_4, expressed by the relation:

$$q_t = q_e - D_1 \exp(-K_1 t) - D_2 \exp(-K_2 t) \quad (3)$$

where D_1 (mg g^{-1}) and K_1 (min^{-1}) are the adsorption rate and diffusion parameter for the fast step, and D_2 and K_2 are those for the slow step. The model is suitable for an adsorbent with two different types of adsorption sites, and the adsorption contains fast and slow adsorption steps.[56,58] The experimental data are fitted by the DEM model at 25, 50, 75 and 100 °C (Fig. 5A). Both D_1 and D_2 first increase, and then decrease with the increase of temperature from 25 to 100 °C, and the highest value appeared at 50 °C (Table S1, ESI†). At 100 and 75 °C, the CO_2 adsorption equilibrium reached within 5 min. With decrease in temperature, the adsorption of CO_2 goes slow on the PEI@Mg_2SiO_4. The slow adsorption is much more obvious at 25 and 50 °C, and the equilibrium has not been reached at 15 min. This demonstrates a strong diffusion of CO_2 is hindered by PEI phase at low temperature,[57] proven by the diffusion parameter (K_1, K_2) (Table S2, ESI†). Evidently, the PEI@Mg_2SiO_4 exhibits the highest adsorption for CO_2 at 50 °C. The kinetic results are also consistent with previous reports.[56] This may provide a valuable application to collect CO_2 from flue gas. In addition, the CO_2 adsorption equilibrium on the PEI@Mg_2SiO_4 is completed in 18 min, while that on the Mg_2SiO_4 is completed in 35 min (Fig. S3, ESI†). The adsorption time is close to other types of adsorbents.[10,56,59,60]

The successive CO_2 adsorption–desorption cycle may provide an assessment of the regeneration stability of the materials. The trend of cycle curves is consistent with that of other studies[53,61,62] (Fig. 5B). During four cycles, the CO_2 capture amounts decrease from 0.94 to 0.75 mmol g^{-1} with PEI@Mg_2SiO_4; however, with Mg_2SiO_4, it decreases, from 0.74 to 0.46 mmol g^{-1}. The CO_2 adsorption capacity of the PEI@Mg_2SiO_4 regenerated decreases by only 15–20%. In addition, from curve 1 more than 18% CO_2 is always left on the Mg_2SiO_4 every cycle. On the contrary, from curve 2 the desorption rate of CO_2 remains more than 91% with the PEI@Mg_2SiO_4.

Prediction of NACs adsorption uptakes in the PEI@Mg_2SiO_4

As described above, the PEI@Mg_2SiO_4 carries a great deal of positive charges. It may adsorb strongly NACs, such as NP, DNP and TNP, *via* electric attraction. Moreover, there are many electron-withdrawing groups (nitro group) in NACs, which are in favour of being adsorbed by the PEI@Mg_2SiO_4. The NP, DNP and TNP are tried to be adsorbed by the PEI@Mg_2SiO_4 hybrid composite, and the adsorption obeys the Langmuir isotherm model (Fig. 6B), $1/q_e = 1/(K_a c_e q_\infty) + 1/q_\infty$. From Table 1, q_∞ value is positively related to lg $K_{o/w}$ value, *e.g.* 2.40 mmol g^{-1} for NP (lg $K_{o/w}$ = 1.91), 2.66 mmol g^{-1} for DNP (lg $K_{o/w}$ = 1.54), 4.85 mmol g^{-1} for TNP (lg $K_{o/w}$ = 2.03), which is superior to the other traditional absorbents.[63–67] The ζ-potential of the hybrid composite approaches +7.29 mV, +6.43 mV and −0.39 mV after adsorption of NP, DNP and TNP, respectively. The ± charge attraction plays a primary role in the adsorption of NACs,[6] *i.e.* PEI embedding into the hybrid composite captured NACs from aqueous solution.

Nitro groups can increase the electronegativity of the phenolic hydroxy groups such that the amino groups of PEI@Mg_2SiO_4 can combine with the phenolic hydroxy groups of NACs more efficiently.[68] Such NACs with more nitro groups often exhibit the higher adsorption capacity. In addition, the electron-withdrawing effect of chlorine group is less than that of nitro groups. Methyl groups can reduce the electronegativity of the phenolic hydroxy groups, which weighs against the combination between the amino groups of the PEI@Mg_2SiO_4 and the phenolic hydroxy groups of *p*-cresol. Therefore, the absorption ability of pollutants from high to low is: TNP > DNP > NP > *p*-chlorophenol > *p*-cresol. The lg(K_a) values of NP, DNP and TNP are calculated to be 2.52, 2.66 and 3.05, respectively, which are superior to their lg $K_{o/w}$. There are many long hydrophobic

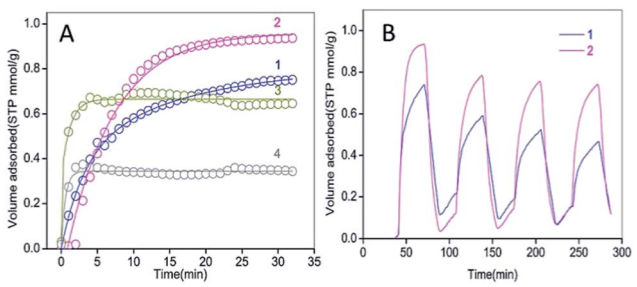

Fig. 5 (A) The CO_2 adsorption kinetics of the PEI@Mg_2SiO_4 at 25 °C (1), 50 °C (2), 75 °C (3) and 100 °C (4) fitting by DEM. (B) Cycles of CO_2 adsorption–desorption for Mg_2SiO_4 (1) and the PEI@Mg_2SiO_4 at 50 °C.

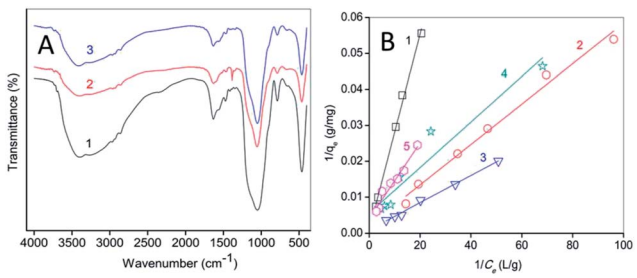

Fig. 6 IR spectra (A) of the PEI@Mg_2SiO_4–NP (1), the PEI@Mg_2SiO_4–DNP (2), the PEI@Mg_2SiO_4–TNP (3), the PEI@Mg_2SiO_4 (4), Mg_2SiO_4 (5) and adsorption of NP (B1), DNP (B2), TNP (B3), *p*-cresol (B4) and *p*-chlorophenol (B5).

Table 1 The adsorption capacity of the PEI@Mg_2SiO_4 to NACs with K_a and comparison with the other sorbents reported

Pollutants	Group category	Nitro groups number, n	q_∞		lg K_a	R^2	q_∞ comparison	
			mmol g^{-1}	mg g^{-1}			Sorbent	q_∞/mg g^{-1}
TNP	Electron-withdrawing	3	4.85	1111	3.05	0.9962	Hydrotalcite	504 (ref. 63)
DNP	groups	2	2.66	455	2.66	0.9884	activated carbon fibers	417 (ref. 64)
NP		1	2.40	333	2.52	0.9763	Granular activated carbon	206 (ref. 65)
p-Chlorophenol		—	2.23	286	2.47	0.9767	—	—
p-Cresol	Electron-donating groups	—	1.68	182	2.26	0.9398	—	—

chains, *i.e.* –$[CH_2–CH_2–N^+]_n$– in PEI, which indicates that PEI@Mg_2SiO_4 carries decent hydrophobicity.[69] Therefore, the hydrophobic interaction occurs between the hydrophobic groups of NACs and the long alkyl chains of embedded PEI in the PEI@Mg_2SiO_4, in addition to the electrical charge interaction.

On the basis of the above experiments, we further carried out *in situ* IR experiments to clarify the NACs kinetics on the adsorbents. *In situ* IR difference spectra upon NACs adsorption, the absorption peaks of nitro groups at 1385–1565 cm^{-1} indicate that NACs are embedded into the hybrid materials (Fig. 6A). The pH of solution affected obviously the adsorption of NACs. With increasing pH from 4 to 6, the q_e of NP and DNP increases by 50% and 215%, respectively, and remains almost constant between pH 7 to 10. The q_e of TNP increases by 20% between pH 4 to 6 and decreases by 37% at pH 10 (Fig. S4, ESI†). The adsorption of NACs increased slightly with increase of ionic strength. This is attributed to the fact that the protonation of PEI is triggered in strong acid.[70] The q_e of NP, DNP and TNP increases by 16%, 4% and 13%, respectively, in 0.25 M NaCl (Fig. S5, ESI†). This is attributed to the fact that ionic strength can strengthen the hydrophobic interaction between NACs and PEI. The adsorption equilibrium is completed in 8 min (Fig. S6, ESI†), which is much faster than that of activated carbon.[71] Therefore, the hybrid sorbent prepared is favorable for treatment of the highly salt and slightly alkaline wastewater.

Conclusions

This work provides a facile layered sorbent (PEI@Mg_2SiO_4) for adsorbing CO_2 and NACs by PEI hybridizing into Mg_2SiO_4. More than 11% PEI is embedded such that the sorbent contains a large numbers of reactive sites to cause an exceptional CO_2 capture capacity. The secondary amine group of PEI with CO_2 plays a key role, and the experimental data fits the DEM. The sorbent exhibits the highest adsorption capacity for CO_2 at 50 °C, *e.g.* approaching 0.94 mmol g^{-1}. The sorbent regenerated by heat treatment exhibits a good stability with the adsorption–desorption cycling of CO_2, *e.g.* decreasing by 20% for four cycles. In addition, the desorption rate of CO_2 remains more than 91% with the PEI@Mg_2SiO_4. Moreover, such a material appears simultaneously multifunctional, *e.g.* adsorption, ionic exchange and flocculation. From the adsorptions of three NACs, the PEI@Mg_2SiO_4 exhibits a high adsorption capacity to NACs, where the electrostatic interaction plays a dominant role. The effect between the electron-donating groups and electron-withdrawing groups plays a supporting role. Then, it adsorbs NP, DNP, and TNP according to the Langmuir isotherm model with a high q_e at 2.40 mmol g^{-1}, 2.66 mmol g^{-1} and 4.85 mmol g^{-1}, respectively. This work may suggest a new strategy for development of CO_2 capture materials and a functionalized material for treatment of NACs wastewater.

Acknowledgements

The authors acknowledge the financial support from the Foundation of State Key Laboratory of Pollution Control and Resource Reuse (Tongji University), China (PCRRK11003).

References

1 S. L. Burkett, A. Press and S. Mann, *Chem. Mater.*, 1997, **9**, 1071–1073.
2 Y. F. Xu, Y. C. Dai, J. Z. Zhou, Z. P. Xu, G. R. Qian and G. Q. M. Lu, *J. Mater. Chem.*, 2010, **20**, 4684–4691.
3 S. N. Britvin, A. Lotnyk, L. Kienle, S. V. Krivovichev and W. Depmeier, *J. Am. Chem. Soc.*, 2011, **133**, 9516–9525.
4 M. V. Jimenez, M. Algarra, J. J. Jimenez and M. Lamotte, *Chemosphere*, 2004, **57**, 179–186.
5 M. J. Manos, V. G. Petkov and M. G. Kanatzidis, *Adv. Funct. Mater.*, 2009, **19**, 1087–1092.
6 Y. P. Wei and H. W. Gao, *J. Mater. Chem.*, 2012, **22**, 5715–5722.
7 G. Decher, *Science*, 1997, **277**, 1232–1237.
8 M. Kimura, R. Sakai, S. Sato, T. Fukawa, T. Ikehara, R. Maeda and T. Mihara, *Adv. Funct. Mater.*, 2012, **22**, 469–476.
9 F. Ciesielczyk, A. Krysztafkiewicz and T. Jesionowski, *J. Mater. Sci.*, 2007, **42**, 3831–3840.
10 L. Estevez, R. Dua, N. Bhandari, A. Ramanujapuram, P. Wang and E. P. Giannelis, *Energy Environ. Sci.*, 2013, **6**, 1785.
11 X. Xue, Q. Gu, G. Pan, J. Liang, G. Huang, G. Sun, S. Ma and X. Yang, *Inorg. Chem.*, 2014, **53**, 1521–1529.
12 H. Cui, Y. Qian, Q. Li, Q. Zhang and J. Zhai, *Chem. Eng. J.*, 2012, **211–212**, 216–223.

13 G. Findenig, R. Kargl, K. Stana-Keinschek and V. Ribitsch, *Langmuir*, 2013, **29**, 8544–8553.
14 Y. Guo, Y. Li, T. Zhu and M. Ye, *Energy Fuels*, 2013, **27**, 360–366.
15 J. Yu, Y. Le and B. Cheng, *RSC Adv.*, 2012, **2**, 6784.
16 R. Wang, S. H. Guan, A. N. Sato, X. Wang, Z. Wang, R. Yang, B. S. Hsiao and B. Chu, *J. Membr. Sci.*, 2013, **446**, 376–382.
17 S. B. Deng and Y. P. Ting, *Environ. Sci. Technol.*, 2005, **39**, 8490–8496.
18 R. Tailor, M. Abboud and A. Sayari, *Environ. Sci. Technol.*, 2014, **48**, 2025–2034.
19 B. J. Gao, P. F. Jiang, F. Q. An, S. Y. Zhao and Z. Ge, *Appl. Surf. Sci.*, 2005, **250**, 273–279.
20 N. Y. Du, H. B. Park, M. M. Dal-Cin and M. D. Guiver, *Energy Environ. Sci.*, 2012, **5**, 7306–7322.
21 D. W. Keith, *Science*, 2009, **325**, 1654–1655.
22 S. Choi, J. H. Drese and C. W. Jones, *ChemSusChem*, 2009, **2**, 796–854.
23 P. Ye and A. T. Lemley, *Water Res.*, 2009, **43**, 1303–1312.
24 N. Dey, S. K. Samanta and S. Bhattacharya, *ACS Appl. Mater. Interfaces*, 2013, **5**, 8394–8400.
25 A. M. Scott, L. Gorb, E. A. Mobley, F. C. Hill and J. Leszczynski, *Langmuir*, 2012, **28**, 13307–13317.
26 P. K. Arora, C. Sasikala and C. V. Ramana, *Appl. Microbiol. Biotechnol.*, 2012, **93**, 2265–2277.
27 A. J. Salter-Blanc, E. J. Bylaska, J. J. Ritchie and P. G. Tratnyek, *Environ. Sci. Technol.*, 2013, **47**, 6790–6798.
28 S. Shi, M. Wang, C. Chen, J. Gao, H. Ma, J. Ma and J. Xu, *Chem. Commun.*, 2013, **49**, 9591–9593.
29 A. Bonnefoy, S. Chiron and A. Botta, *Environ. Toxicol.*, 2012, **27**, 321–331.
30 Q. Wang, H. H. Tay, Z. Y. Zhong, J. Z. Luo and A. Borgna, *Energy Environ. Sci.*, 2012, **5**, 7526–7530.
31 G. G. Qi, Y. B. Wang, L. Estevez, X. N. Duan, N. Anako, A. H. A. Park, W. Li, C. W. Jones and E. P. Giannelis, *Energy Environ. Sci.*, 2011, **4**, 444–452.
32 D. H. Zhao, Y. L. Shen, Y. L. Zhang, D. Q. Wei, N. Y. Gao and H. W. Gao, *J. Mater. Chem.*, 2010, **20**, 3098–3106.
33 P. J. E. Harlick and A. Sayari, *Ind. Eng. Chem. Res.*, 2007, **46**, 446–458.
34 R. Serna-Guerrero, Y. Belmabkhout and A. Sayari, *Chem. Eng. J.*, 2010, **158**, 513–519.
35 G. P. Knowles, S. W. Delaney and A. L. Chaffee, *Ind. Eng. Chem. Res.*, 2006, **45**, 2626–2633.
36 X. L. Ma, X. X. Wang and C. S. Song, *J. Am. Chem. Soc.*, 2009, **131**, 5777–5783.
37 C. Chen, S. T. Yang, W. S. Ahn and R. Ryoo, *Chem. Commun.*, 2009, 3627–3629.
38 M. B. Yue, Y. Chun, Y. Cao, X. Dong and J. H. Zhu, *Adv. Funct. Mater.*, 2006, **16**, 1717–1722.
39 J. T. Wang, D. H. Long, H. H. Zhou, Q. J. Chen, X. J. Liu and L. C. Ling, *Energy Environ. Sci.*, 2012, **5**, 5742–5749.
40 S. M. Lee and D. Tiwari, *Appl. Clay Sci.*, 2012, **59–60**, 84–102.
41 S. K. Parida, S. Dash, S. Patel and B. K. Mishra, *Adv. Colloid Interface Sci.*, 2006, **121**, 77–110.
42 T. Kumeria, A. Santos and D. Losic, *ACS Appl. Mater. Interfaces*, 2013, **5**, 11783–11790.
43 C. S. Cheng, J. Deng, B. Lei, A. He, X. Zhang, L. Ma, S. Li and C. Zhao, *J. Hazard. Mater.*, 2013, **263**, 467–478.
44 D. Suteu, A. C. Blaga, M. Diaconu and T. Malutan, *Cent. Eur. J. Chem.*, 2013, **11**, 2048–2057.
45 F. Rezaei, R. P. Lively, Y. Labreche, G. Chen, Y. Fan, W. J. Koros and C. W. Jones, *ACS Appl. Mater. Interfaces*, 2013, **5**, 3921–3931.
46 J. Y. Kim, J. Kim, S. T. Yang and W. S. Ahn, *Fuel*, 2013, **108**, 515–520.
47 S. L. Burkett, A. Press and S. Mann, *Chem. Mater.*, 1997, **9**, 1071–1073.
48 A. Zukal, I. Dominguez, J. Mayerova and J. Cejka, *Langmuir*, 2009, **25**, 10314–10321.
49 S. T. Yang, J. Y. Kim, J. Kim and W. S. Ahn, *Fuel*, 2012, **97**, 435–442.
50 J. Yu, S. Liu and H. Yu, *J. Catal.*, 2007, **249**, 59–66.
51 N. P. Wickramaratne and M. Jaroniec, *J. Mater. Chem. A*, 2013, **1**, 112.
52 M. M. Gui, Y. X. Yap, S.-P. Chai and A. R. Mohamed, *Int. J. Greenhouse Gas Control*, 2013, **14**, 65–73.
53 S. B. Yang, L. Zhan, X. Y. Xu, Y. L. Wang, L. C. Ling and X. L. Feng, *Adv. Mater.*, 2013, **25**, 2130–2134.
54 Q. Wang, Y. S. Gao, J. Z. Luo, Z. Y. Zhong, A. Borgna, Z. H. Guo and D. O'Hare, *RSC Adv.*, 2013, **3**, 3414–3420.
55 A. Chakradhar and U. Burghaus, *Surf. Sci.*, 2013, **616**, 171–177.
56 Z. Chen, S. Deng, H. Wei, B. Wang, J. Huang and G. Yu, *ACS Appl. Mater. Interfaces*, 2013, **5**, 6937–6945.
57 P. Bollini, N. A. Brunelli, S. A. Didas and C. W. Jones, *Ind. Eng. Chem. Res.*, 2012, **51**, 15153–15162.
58 N. Chiron, R. Guilet and E. Deydier, *Water Res.*, 2003, **37**, 3079–3086.
59 Z.-h. Tang, Z. Han, G.-z. Yang, B. Zhao, S.-l. Shen and J.-h. Yang, *New Carbon Mater.*, 2013, **28**, 55–60.
60 F. Durán-Muñoz, I. C. Romero-Ibarra and H. Pfeiffer, *J. Mater. Chem. A*, 2013, **1**, 3919.
61 A. Garcia-Gallastegui, D. Iruretagoyena, M. Mokhtar, A. M. Asiri, S. N. Basahel, S. A. Al-Thabaiti, A. O. Alyoubi, D. Chadwick and M. S. P. Shaffer, *J. Mater. Chem.*, 2012, **22**, 13932–13940.
62 A. Garcia-Gallastegui, D. Iruretagoyena, V. Gouvea, M. Mokhtar, A. M. Asiri, S. N. Basahel, S. A. Al-Thabaiti, A. O. Alyoubi, D. Chadwick and M. S. P. Shaffer, *Chem. Mater.*, 2012, **24**, 4531–4539.
63 M. C. Hermosin, I. Pavlovic, M. A. Ulibarri and J. Cornejo, *Water Res.*, 1996, **30**, 171–177.
64 Q. S. Liu, T. Zheng, P. Wang, J. P. Jiang and N. Li, *Chem. Eng. J.*, 2010, **157**, 348–356.
65 A. Kumar, S. Kumar and D. Gupta, *J. Hazard. Mater.*, 2007, **147**, 155–166.
66 M. G. Roberts, C. L. Rugh, H. Li, B. J. Teppen and S. A. Boyd, *Environ. Sci. Technol.*, 2007, **41**, 1641–1645.
67 T. B. Hofstetter, R. P. Schwarzenbach and S. B. Haderlein, *Environ. Sci. Technol.*, 2003, **37**, 519–528.

68 A. Reynal, A. Forneli, E. Martinez-Ferrero, A. Sanchez-Diaz, A. Vidal-Ferran, B. C. O'Regan and E. Palomares, *J. Am. Chem. Soc.*, 2008, **130**, 13558–13567.
69 M. Amara and H. Kerdjoudj, *Desalination*, 2003, **155**, 79–87.
70 F. An, B. Gao and X. Feng, *J. Hazard. Mater.*, 2008, **157**, 286–292.
71 A. A. M. Daifullah and B. S. Girgis, *Water Res.*, 1998, **32**, 1169–1177.